Journal of Sailboat Technology, Article 2010-01.

EXPERIMENTAL STUDY OF THE HYDRO-IMPACT OF SLAMMING IN A MODERN RACING SAILBOAT

June Lee
Department of Ocean Systems Engineering, KAIST, Korea.

Philip A. Wilson
Fluid Structure Interaction Group, University of Southampton, UK.

Manuscript received September 16, 2008; revision received May 8, 2009; accepted August 26, 2009.

Abstract: The hydrodynamic impact, or hydro-impact, phenomenon caused by slamming on racing yachts and the local structure's response is studied experimentally. Pressure transducers and a special measurement system named 'Slam Patch' have been designed and implemented to measure the hydro-impact pressure and/or the local structure's response. The measurement systems were installed on a 1/7-scale model of an Open 60 yacht. Modal, rotational drop, and seakeeping-slamming tests are carried out. The measured hydro-impact pressure was processed statistically. A methodology to scale up the test results to prototype is mentioned. At the same time, the transient response of a simple structure under half-sine impulse is calculated using a commercial finite element analysis program to study the effect of the relationship between impulse duration and natural frequency of the structure.

Keywords: design, experimental methods, hull, hydrodynamics, model testing, slamming, structures.

NOMENCLATURE

FRF	Frequency Response Function
H_D	Drop height
H_w	Wave height
P/D	Probability Distribution
P_{EX}	Extreme peak pressure
P_P	Peak pressure
P/T	Pressure Transducer
Q_I	Impulse quantity
S/P	Slam Patch
T_D	Duration time
T_R	Rise time
V	Speed of boat

INTRODUCTION

Weight is a governing factor for the speed of a racing yacht. To maximize speed optimization of the structure is key whether the race area has calm water like the America's Cup or the severe sea of the Southern Ocean as in the Vendée globe or Volvo Ocean Race. Although the speed of racing boats increases through the use of light and stiff material, structural damage by slamming is still significant as reported by Bunting and Sheahan (2009). It is expected that the structural damage may be influenced by global hydro-elastic behaviour from waves and/or local hydro-impact from slamming.

Starting with the work of von Karman (1929), various research works have been carried out in naval architecture (Ochi and Motter, 1973; Faltinsen, 2000; Kapsenberg et. al., 2003), on motorboats (Heller and Jasper, 1961; Stavovy and Chuang, 1976; Savitsky and Brown, 1976; Allen et. al., 1978), and on sailboats (Joubert, 1982; Reichard, 1984; Hentinen and Holm, 1994; Joubert, 1996) in parallel with rules and regulations (ABS, 1994; ISO, 2008; BV, 2008). Nonetheless, as pointed out by Manganelli (2006), and Bunting and Sheahan (2009), a growing number of engineers and researchers agree on the need for more accurate knowledge of the hydro-impact problem in sailboats as new problems appear due to the continuously enhanced performance of sailboats. In this regard, hydro-impact in the waves during slamming is the subject of this study.

First, a specially built measurement system named 'slam patch' is designed and implemented with pressure transducers on a model boat and a series of hydro-impact tests are carried out. This slam patch system, which is based on force transmissibility, is designed to represent the local structure of the boat and/or a simple pressure/force transducer as a transition device between the pressure transducer and strain gauge. It is found that the slam patch system can be implemented to measure the total response of the local structure which can be divided into two components – hydro-impact load and vibration behaviour of the local structure under fluid-structure interaction.

Second, various measurement systems are installed in a scale model of an Open 60 and hydro-impact tests are carried out – a rotational drop test and a seakeeping-slamming test. In the drop test, it is found that as drop height increases, which means impact velocity increases, the transient response of the structure is significant and far exceeds the magnitude of the hydro-impact load itself measured at the pressure transducer. This is due either to the existence of resonance of the structure or the location of the pressure transducer, which is at the perimeter of the slam patch or sampling rate limitation. In the seakeeping-slamming test, because of the limitation of wave height, a maximum wave of 0.2 m was used in scale model to find the hydro-impact load. It was found that with a wave height of 0.2 m, the measured response of the slam patch system was pure hydro-impact load or slightly coupled with the structure's resonance. The measured signals were processed statistically to predict the general trend of the hydro-impact phenomenon.

DESIGN OF SLAM PATCH SYSTEM

Various instruments can measure the hydro-impact load – pressure transducer, pressure panel, strain gauge, or accelerometer. Each instrument has its own advantages and disadvantages. For example, a pressure transducer can measure exact pressure at a given point but can miss the highest pressure value. A strain gauge and accelerometer can measure the total response of a structure when the structure impacts the fluid; however, the hydro-impact load from the fluid cannot be inferred when the exact response of the structure is unknown. The concept of the slam patch system, which belongs to the pressure panel category, is to measure the impact load by the fluid and/or to measure the response of the local structure. To design the system, the duration and the peak pressure of the hydro-impact caused by slamming must be known so the components of net hydro-impact load and response of structure can be either separated or coupled.

In the study of Manganelli et. al. (2003), a slam patch system is configured to find the hydro-impact load and hydro-elastic effect. In their study, the slam patch system is assumed as a 1-DOF system. The 80 by 80 mm slam patch is designed and tested in dry

and wet modes[1]. It is found that in dry mode the linear range before the first resonance is between 300 Hz and 400 Hz. The corresponding linear range in wet mode is 200 Hz. After the slamming tests, hydro-impact signals are filtered to eliminate the resonant response of the slam patch system.

In this study, the dynamic behaviour of the slam patch system is investigated to a further degree. Figure 1 shows the slam patch system used in this study.

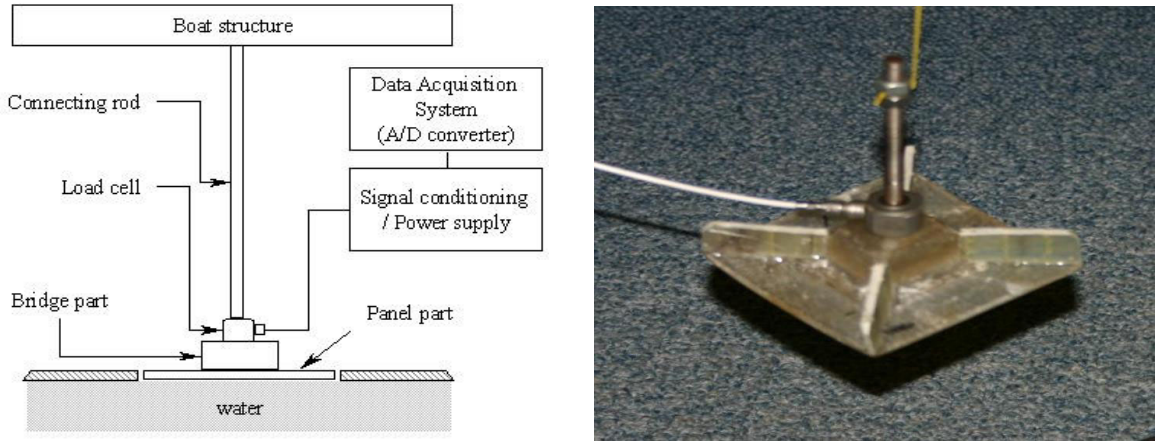

Figure 1. Slam patch system (left: schematic, right: prototype)

To ensure that the frequency range of the hydro-impact load is not near the resonance of the slam patch system, the boundary where the system is attached is reinforced. Numerical calculation and modal testing are carried out to measure the force transmissibilities in dry and wet modes. In the modal testing direct and transfer FRF's are obtained. However, in the wet mode direct FRF is impossible to obtain, only transfer FRF's are compared as shown in Figure 2.

[1] Dry mode: when the structure is in vacuo, wet mode: when the structure is in or on water.

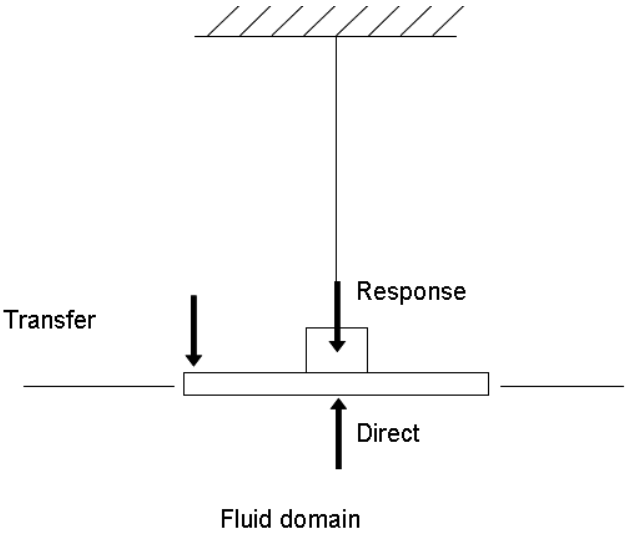

Figure 2. Measurement in modal testing

It is found that the slam patch system behaves like a cantilever beam with a mass at the free end, which is shown in equations (1), (2) and Figure 3.

$$2\pi f_T = \omega_T = \sqrt{k_T / m_{eqT}} = \sqrt{\frac{3EI/L^3}{M + 0.23m}} \qquad (1)$$

$$2\pi f_L = \omega_L = \sqrt{k_L / m_{eqL}} = \sqrt{\frac{EA/L}{M + 0.33m}} \qquad (2)$$

where:

f, ω =	frequency in Hz and rad/sec, respectively.
k_T, k_L =	effective stiffness of beam in transverse and longitudinal directions, respectively.
m_{eqT}, m_{eqL} =	effective mass in transverse and longitudinal directions, respectively.
M, m =	mass at the free end of beam and mass of beam, respectively.
E =	Young's modulus of beam.
A =	section area of beam.
I =	moment of inertia of beam section.
L =	length of beam.

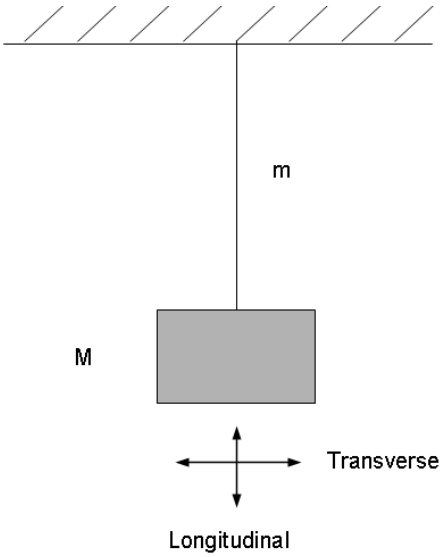

Figure 3. Cantilever beam with a mass at the free end

In the numerical calculation the natural frequencies are 481, 580, 593, and 1343 Hz in dry mode and 345, 371, 535, and 805 Hz in wet mode. After modal testing, the acceptable linear ranges where force transmissibility is unity (= 1) are up to 500 Hz in dry mode and up to 250 Hz in wet mode. Figure 4 shows one (slam patch No. 3) of the transfer force transmissibilities of six slam patches in dry and wet modes. In the figures of dry and wet mode, each line is the transmissibility from one impact test whereas the bold line is the average transmissibility.

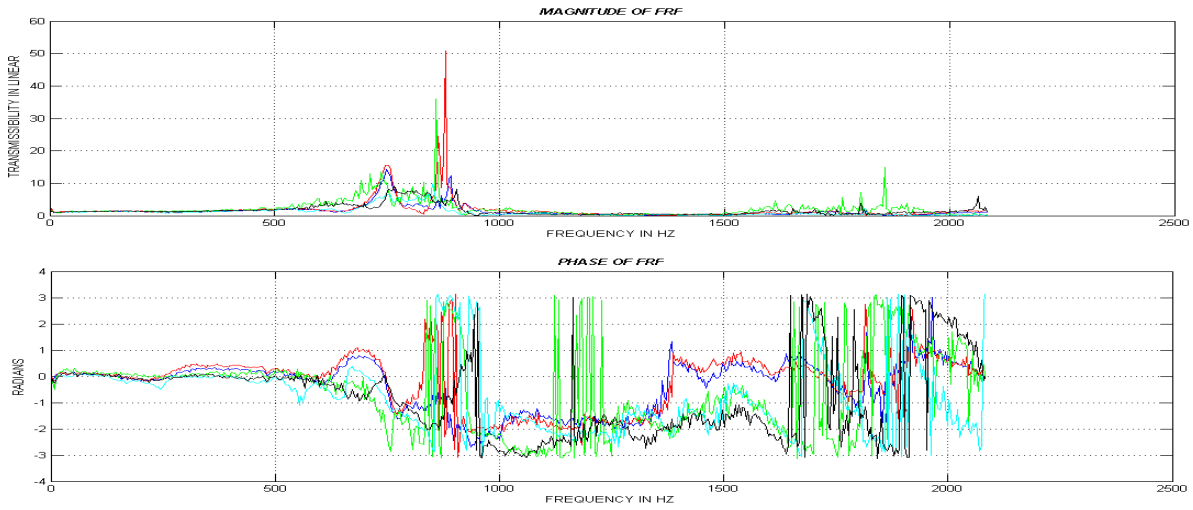

(a) Slam patch 3 in dry mode

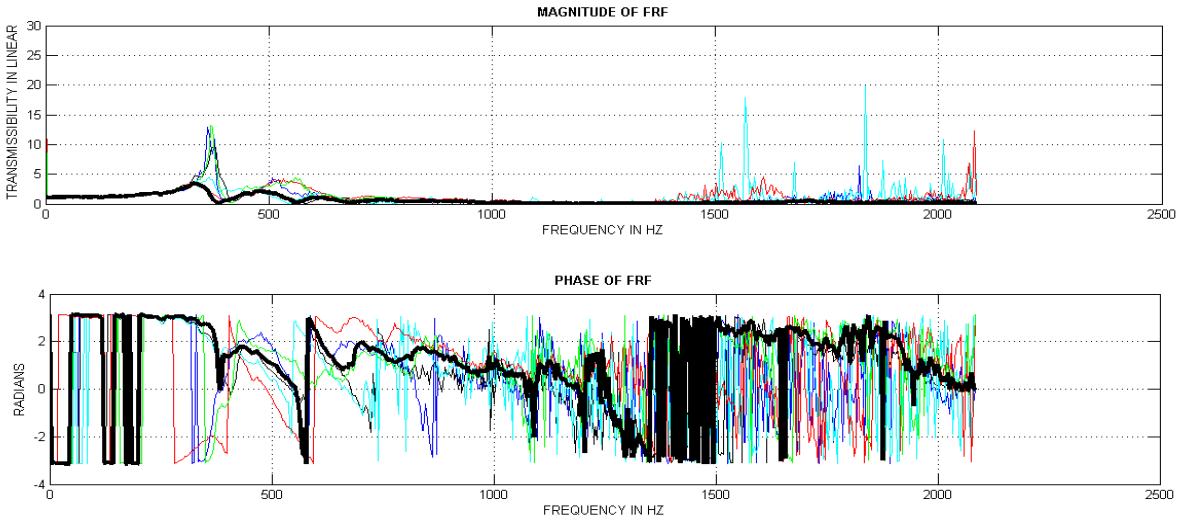

(b) Slam patch 3 in wet mode

Figure 4. Force transmissibility (transfer FRF's) of slam patch No. 3

ROTATIONAL DROP TEST

The objectives of the rotational drop test are:

- To assess the behaviour of the slam patch when measuring the hydro-impact load.
- To measure the hydro-impact load and/or the response of the local structure with regard to drop height.

The test is carried out with a 1/7-scale model of an Open 60 yacht in calm water with three slam patch systems, four pressure transducers, one potentiometer, and one accelerometer installed on the fore body of the model. Figure 5 and Table 1 show the details of the yacht in this study.

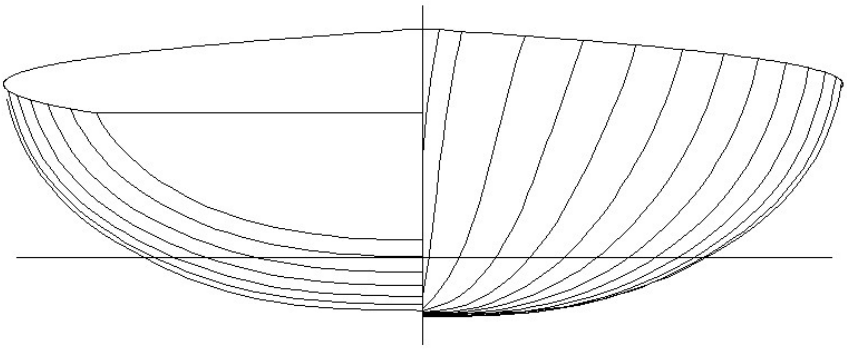

Figure 5. Body plan of Open 60 (Finot-Conq design, France)

Table 1. Principal characteristics of Open 60 (Finot-Conq design, France)

Principals	Values
Displacement	11,290 (kg)
LWL	16.968 (m)
BWL	3.89 (m)
Draught (bare hull)	0.405 (m)
Deadrise angle at 0.5 LWL (Station 5)	20, 7.5, 4.5[2] (degree)

The fundamental hardware configuration in the drop test and the seakeeping-slamming test are given in Table 2.

Table 2. Key hardware

Item	Model	Remark
A/D converter	PCM-DAS08	24 kHz
DAQ system	Labview 8.0 Turboad	Sampling rate: 3125 Hz Sampling rate: 1512 Hz
Slam patch	In house made	± 40 kPa
Pressure transducer	RDP A105	344.7 kPa
Amplifier	RDP 600	
Accelerometer	Endevco 2256	± 50 g
Potentiometer	In house made	

The locations of measurement and set up in the drop test are shown in Figure 6. The accelerometer is attached to the reinforcement structure over slam patch 2.

[2] By the definitions of ISO, BV and DNV respectively; however, the local deadrise angles at the bottom area where the slam patches are installed are flat, i.e. 0º.

(a) Test set up

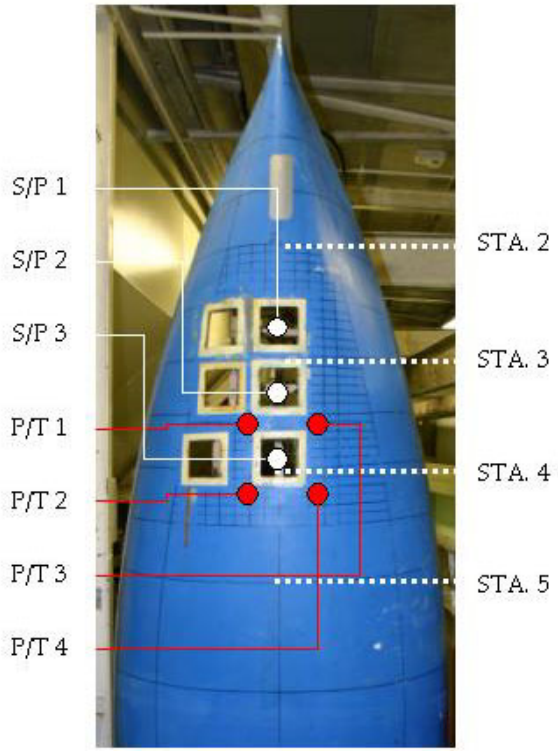

(b) Instrument installation

(c) Instrument installation

Figure 6. Rotational drop test set up

Figure 7 is a typical result of the drop test where, around the four corners of slam patch 3 (slam patch 380), four pressure transducers are installed. In this case, the drop height is 4 cm from the bottom of slam patch 3 (slam patch 380) to the water surface.

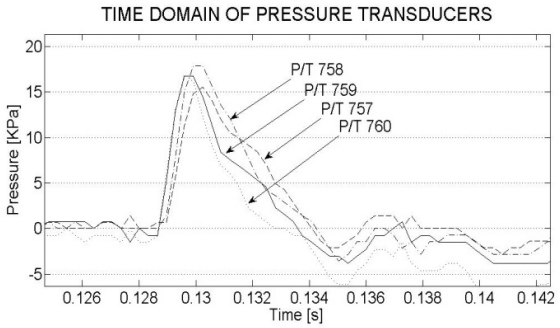

(a)Time histories of P/T's

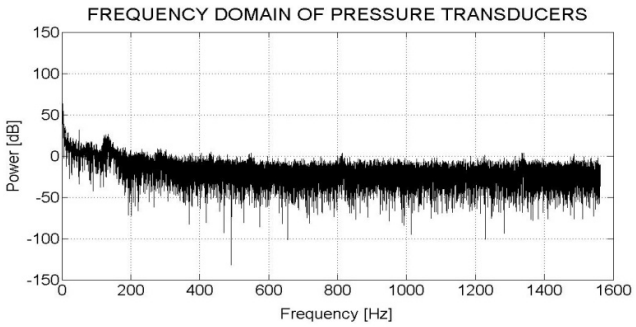

(b) Power spectrums of P/T's

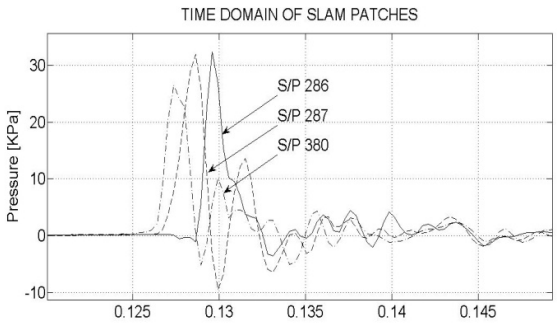

(c) Time histories of S/P's

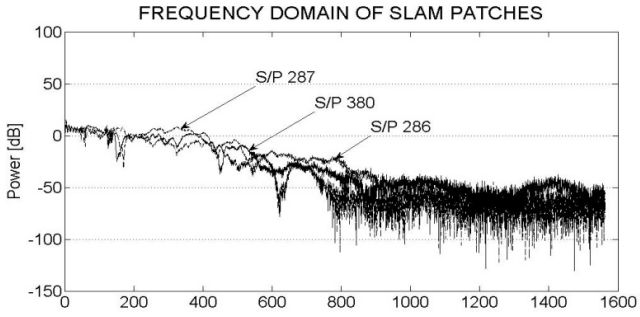

(d) Power Spectrums of S/P's

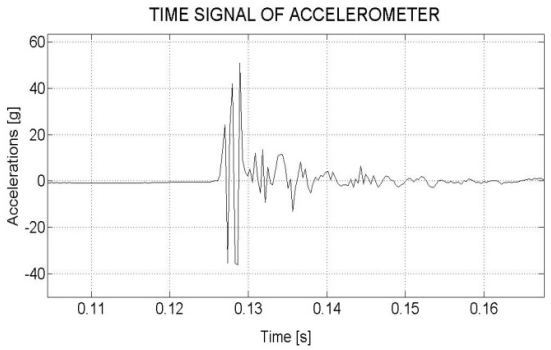

(e) Time history of accelerometer

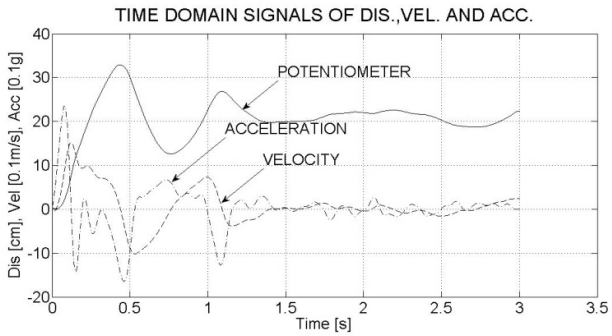

(f) Time history at potentiometer

Figure 7. Typical test result (drop height = 0.04 m)

Note that the magnitude and power of the accelerometer is extremely high, over 40 g. Consistent results are acquired during the other drop height where the pressure at the slam patch is greater than the pressure at the pressure transducer. This is due to either the dynamic load factor (resonance) of the structure being within the range of excitation, or the pressure transducer being located at the perimeter of slam patch such that the first highest impact occurs at the slam patch; however, the perimeter assumption can be rejected since the three slam patches show a similar degree of pressure shown in (c) of Figure 7.

On the other hand, since it is recommended that at least a 20 kHz sampling rate is needed to measure the hydro-impact signals in pressure transducers (Campbell and Weynberg,

1979; Wraith, 1998; Kwon et. al., 2005), the possibility of missing the peak at a pressure transducer cannot be excluded because of the relatively low sampling rate of 3125 Hz.

In the series of drop and sloshing tests by Kwon et al. (2005), it was found that at a sampling rate of over 20 kHz extraordinary high peak pressure which was undetected at the low sampling rate was found. Thus, pressure transducers underestimate the original signals of impact pressure in this case. Figure 8 supports the former case where the structure is flexible enough that the dynamic load factor or resonance plays a significant role. It shows a typical hydro-impact force and its power spectrum density as the drop height increases.

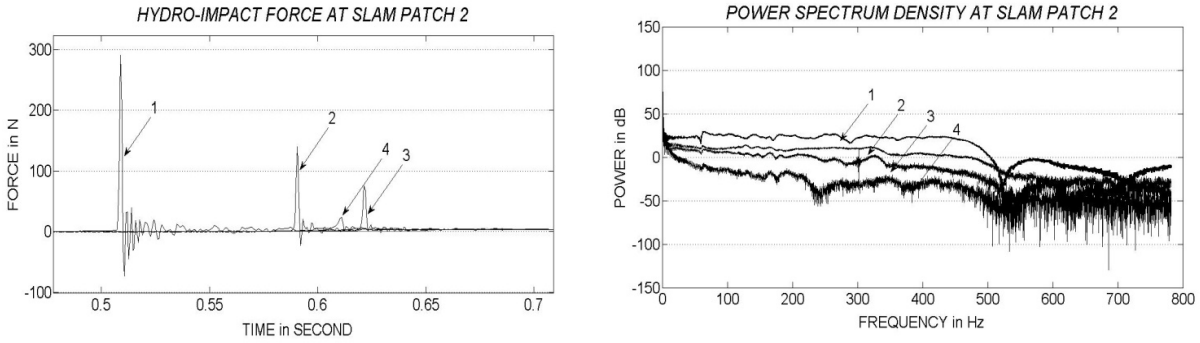

(a) Time history of hydro-impacts **(b) Corresponding power spectra**

Figure 8. Four hydro-impacts (1~4) and corresponding power spectra

No. 4 in Figure 8 is the case of the lowest drop height where the hull bottom just touches the water by surface tension effect. No. 1 is the case of the highest height of 0.4 m where the signal is clipped off - the maximum capacity of the slam patch system is 290 N (nominal capacity is 250 N). As the drop height increases, the range of frequency that contributes to the power of the hydro-impact also increases. This means that as the drop height increases, the response of the structure includes the components of resonance of the structure due to the extended frequency range.

Figure 9 shows the relationships between various variables in the drop test. The data are fitted by 1st and 2nd degree polynomials.

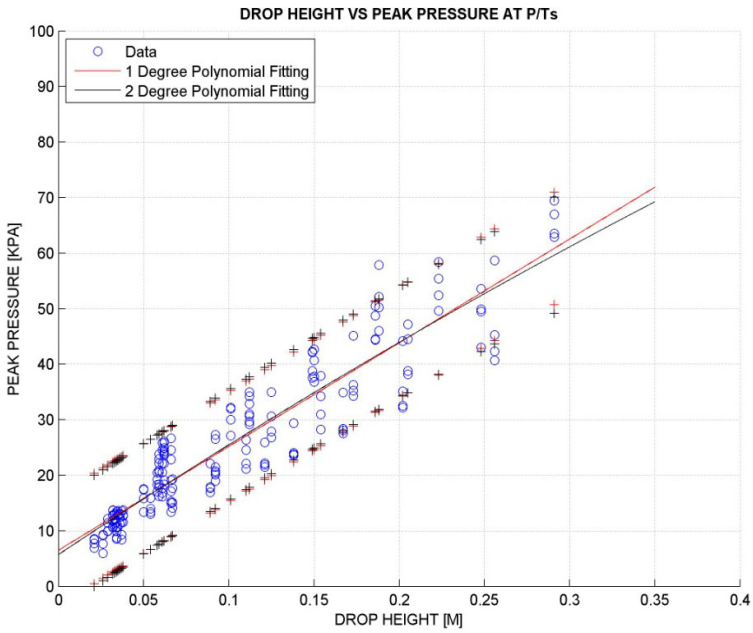

(a) P_p vs H_D at P/T's

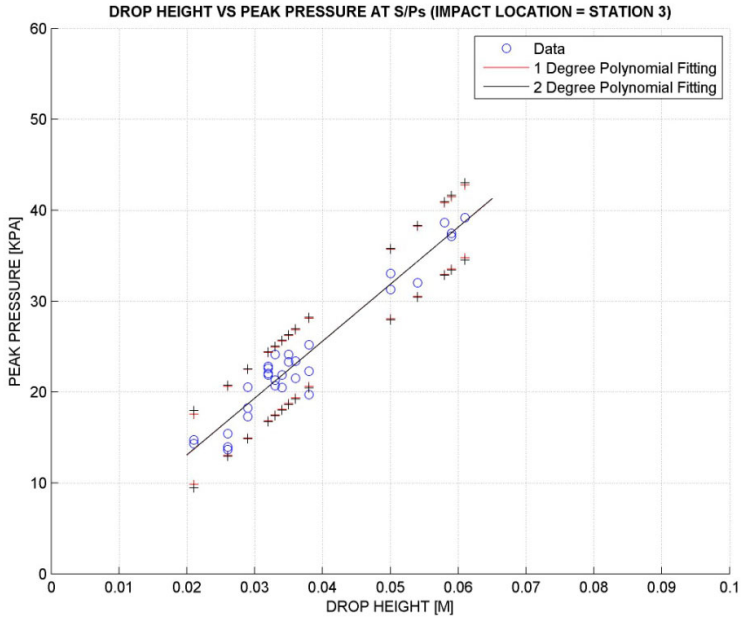

(b) P_p vs H_D S/P's

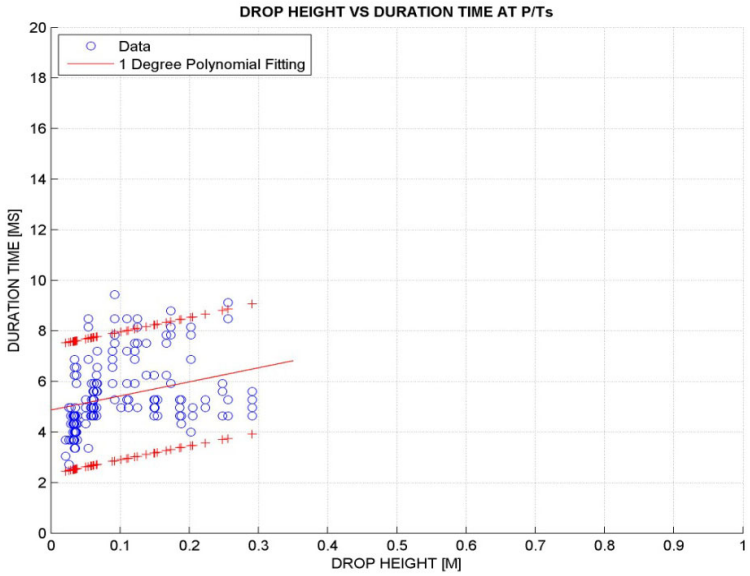

(c) T_D vs H_D at P/T's

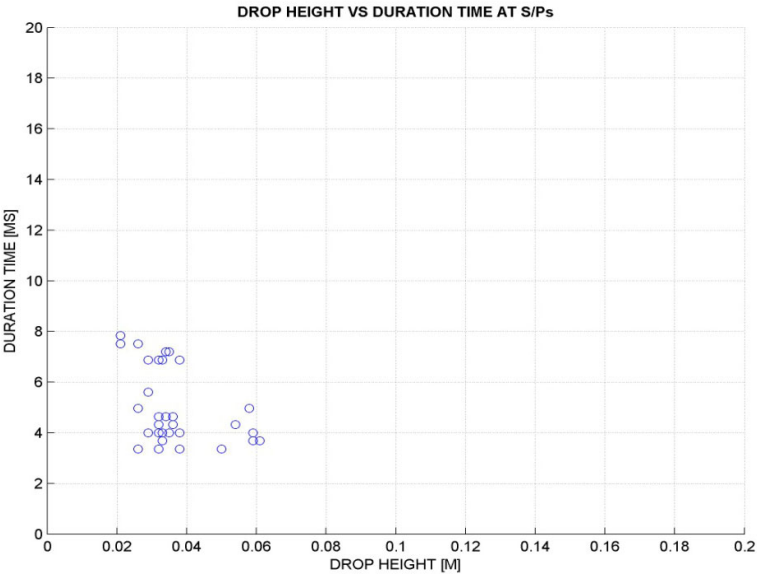

(d) T_D vs H_D at S/P's

Figure 9. Hydro-impact characteristics in drop test

The peak pressure has a linear relationship to drop height for both the pressure transducers and slam patches as shown in Figure 9 (a) and (b). Although the relationship between peak pressure and impact velocity is omitted, it also has a linear relationship since the impact velocity is the function of drop height. Duration time is an important factor in the calculation of the structural response to the impulse. In this case, both pressure transducers and slam patches show a converging tendency as the drop height increases as shown at the Figure 9 (c) and (d), even though it is interpolated by a linear function

because of the scarcity of the data. This will be investigated further in the seakeeping-slamming test below.

In this drop test, it is found that:

- Low pressure is detected at the pressure transducer because of the low sampling rate limit.
- As the drop height increases, magnification is dominant in the slam patch. However, at present, it is difficult to detect the fluid-structure interaction effect (for example, reduction of peak pressure), because there is no evidence with regard to the response of the slam patch in vacuo when the same impact load is applied.

SEAKEEPING-SLAMMING TEST

A series of seakeeping-slamming tests are carried out in regular waves. The test matrix is given in Table 3, where wave frequency (f_w), wave height (H_w), and boat speed (V) are parameters. The measurement location is shown at Figure 10 (a) where the slam patches are lined up on the centre of the fore-body (station 2.5 to 4) of the model. In contrast to the drop test, the sensors are distributed to determine the longitudinal distribution of the hydro-impact pressure.

Table 3. Seakeeping-slamming test matrix

Item	Model scale	Full scale
Wave frequency (f_w)	0.4 ~ 0.95 Hz with 0.05 Hz increment	0.15 ~ 0.36 Hz
Wave height (H_w)	0.1/ 0.15/ 0.2 m	0.7/ 1.05/ 1.4 m
Boat speed (V)	1.5/ 2/ 2.5 m/s	7.7/ 10.3/ 12.8 knots

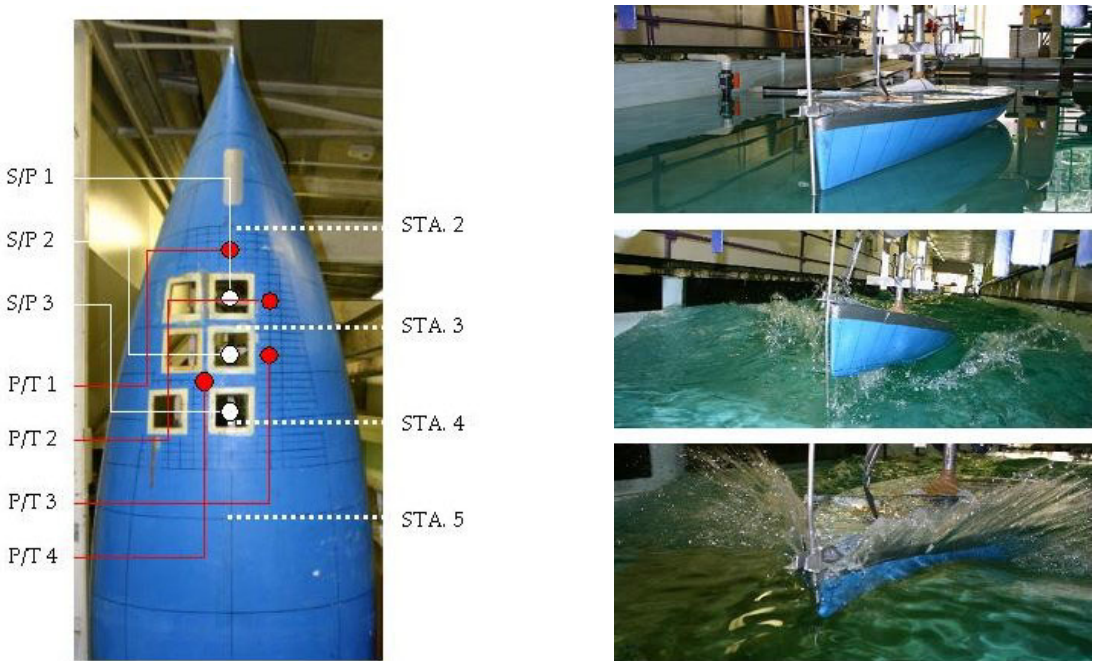

(a) Measurement location **(b) Testing**

Figure 10. Seakeeping-slamming test set up

At specific locations

In the seakeeping-slamming test, the foremost area shows the greatest peak pressure consistently throughout the test matrix. The hydro-impact pressures measured at the slam patch are well within the capacity of the slam patch, which implicitly means that the drop height or impact velocity is relatively smaller than in the drop test. The results at the foremost area of pressure transducer 1 and slam patch 1 are processed statistically and presented in Figure 11 as the relationship based on various boat speeds.

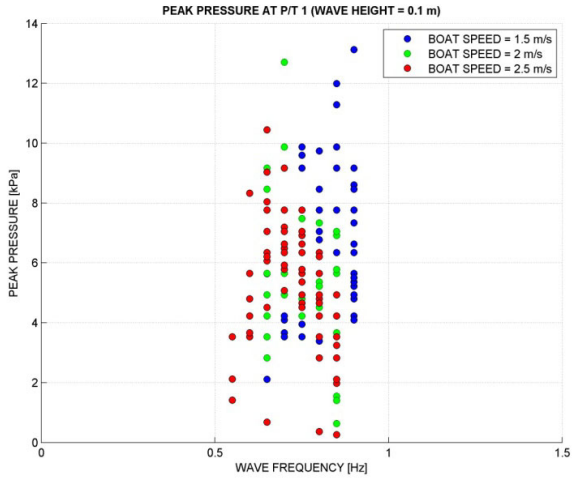

(a) Pp distribution at Hw = 0.1 m (P/T 1)

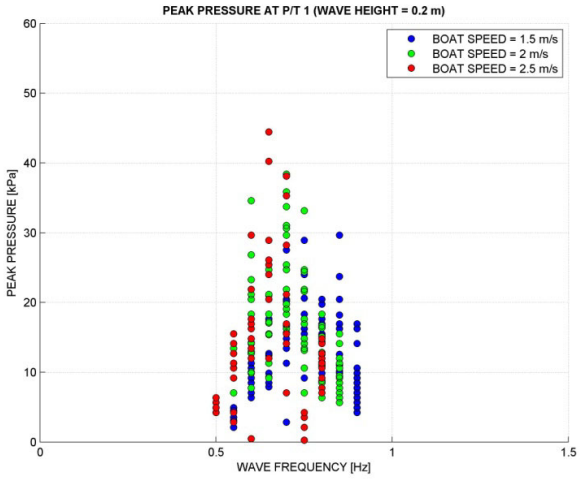

(b) Pp distribution at Hw = 0.2 m (P/T1)

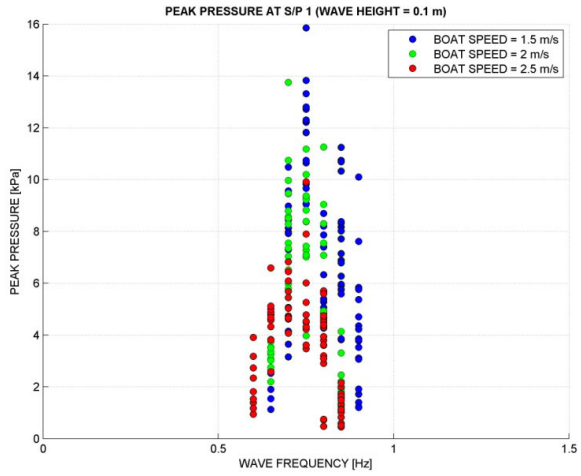

(c) P_p distribution at H_w = 0.1 m (S/P 1)

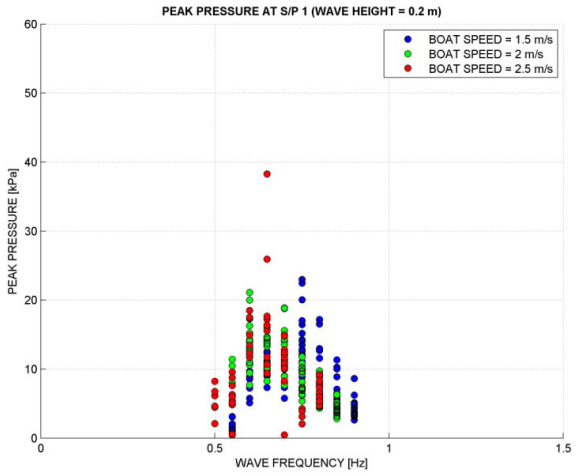

(d) P_p distribution at H_w = 0.2 m (S/P 1)

Figure 11. Peak pressure (P_p) vs wave frequencies at P/T 1 and S/P 1 at wave height (H_w) of 0.1 and 0.2 m in seakeeping-slamming test

In these test results, significant hydro-impact pressures are detected at:

- The wave frequency of 0.65 ~ 0.75 Hz,
- The foremost area of pressure transducer 1 and slam patch 1,
- The higher wave height of 0.2 m.

Figure 12 and Figure 13 are the corresponding histograms and probability distributions of pressure transducer 1 (P/T1) and slam patch 1 (S/P1) at the specific wave height and boat speed. The histograms are fitted by Gamma and Weibull distribution functions. The Gamma distribution shows a slightly better fit throughout the histograms (i.e., has a greater maximum likelihood of 1% and a smaller variance of 3% than the Weibull distribution in goodness-to-fit analysis).

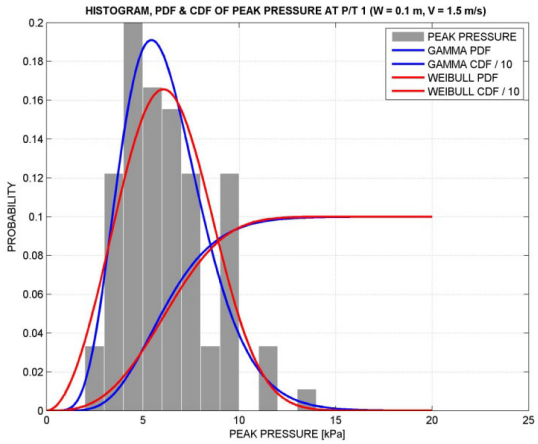

(a) Hw=0.1 m, V=1.5 m/s

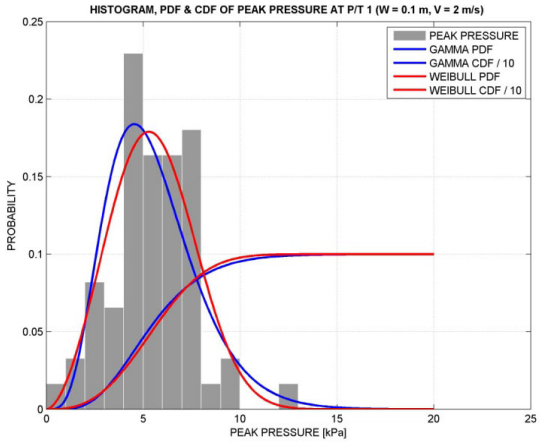

(b) Hw =0.1 m, V =2.0 m/s

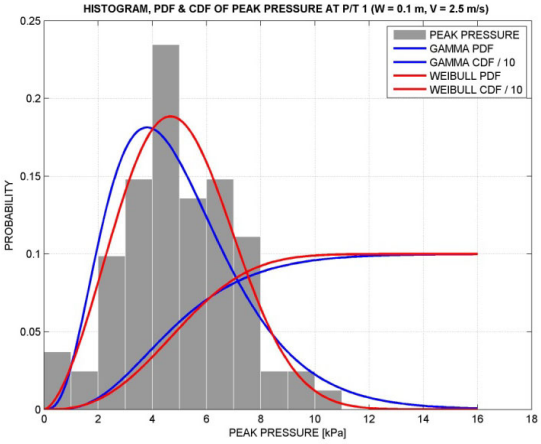

(c) H_w =0.1 m, V =2.5 m/s

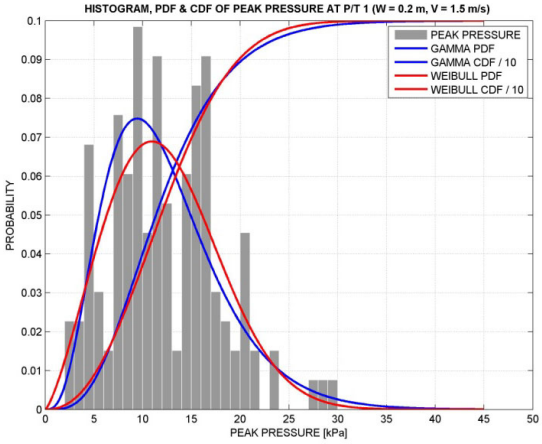

(d) H_w =0.2 m, V =1.5 m/s

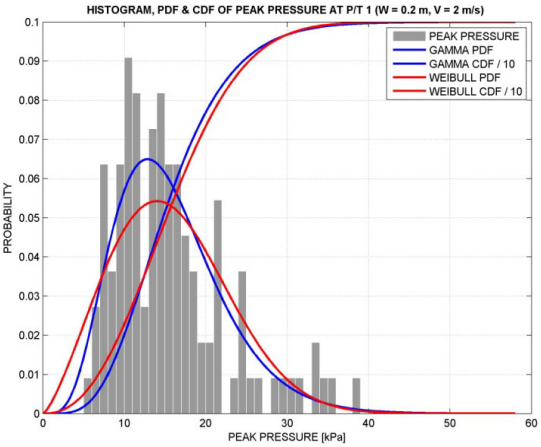

(e) Hw =0.2 m, V =2.0 m/s

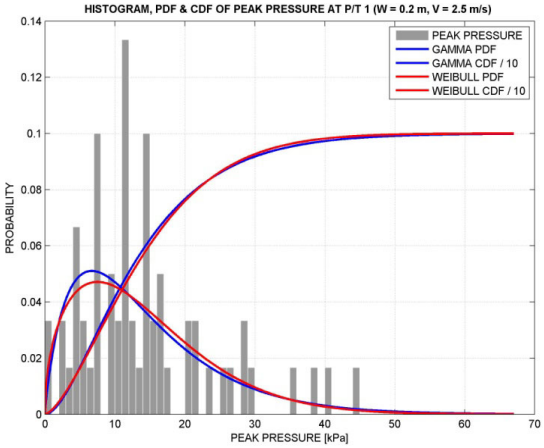

(f) Hw =0.2 m, V =2.5 m/s

Figure 12. Histogram and probability of P/T 1 in seakeeping-slamming test

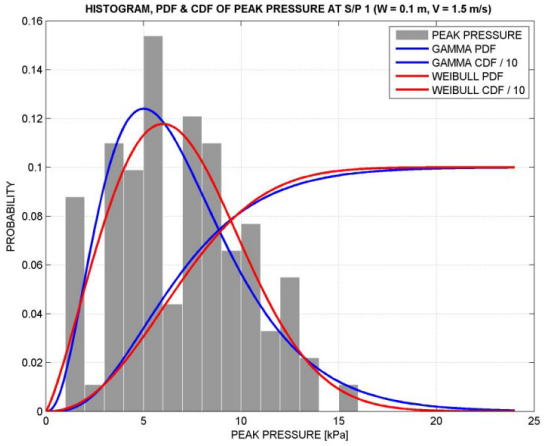

(a) Hw =0.1 m, V =1.5 m/s

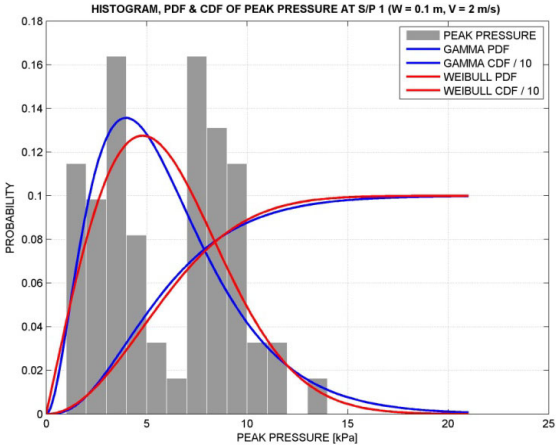

(b) Hw =0.1 m, V =2.0 m/s

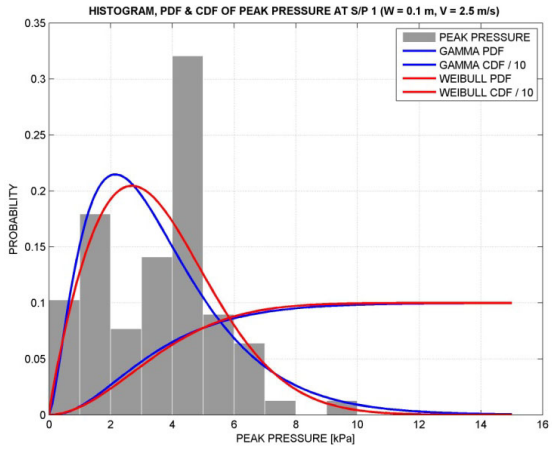

(c) Hw =0.1 m, V =2.5 m/s

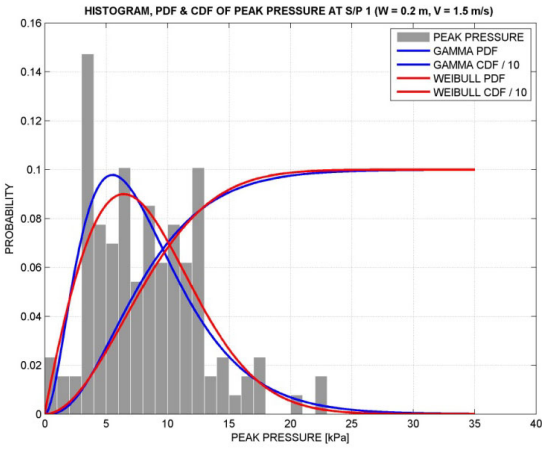

(d) Hw =0.2 m, V =1.5 m/s

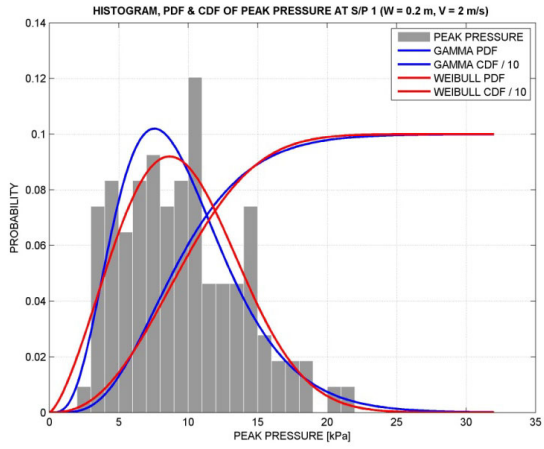

(e) Hw =0.2 m, V =2.0 m/s

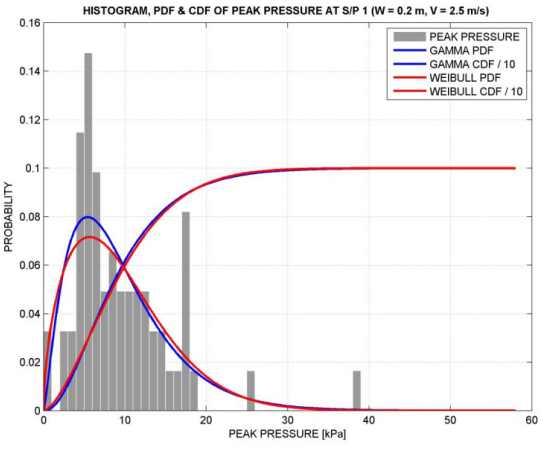

(f) Hw =0.2 m, V =2.5 m/s

Figure 13. Histogram and probability of S/P 1 in seakeeping-slamming test

The highest peak pressure is not necessarily a function of boat speed in the case of a wave height of 0.1 m, whereas a wave height of 0.2 m shows the opposite situation where the highest peak pressure depends on the boat speed.

At all locations in the entire test matrix

In the previous section, pressure transducer 1 and slam patch 1 showed the highest and most significant hydro-impact pressure. Figure 14 shows the hydro-impact characteristics at all locations within the entire test matrix. By doing so, the hydro-impact characteristics such as peak pressure (P_p), duration time (T_D), rise time (T_R), and impulse quantity (Q_I) in the bottom area of the model can be traced.

In (a) and (b) of Figure 14, it is confirmed that pressure transducer 1 and slam patch 1 show the highest distribution of the peak pressure. As the peak pressure increases, the duration time and rise time converge.

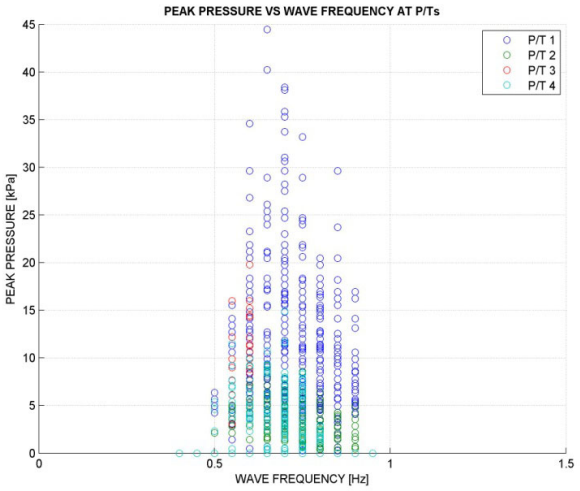

(a) P_p at P/T's

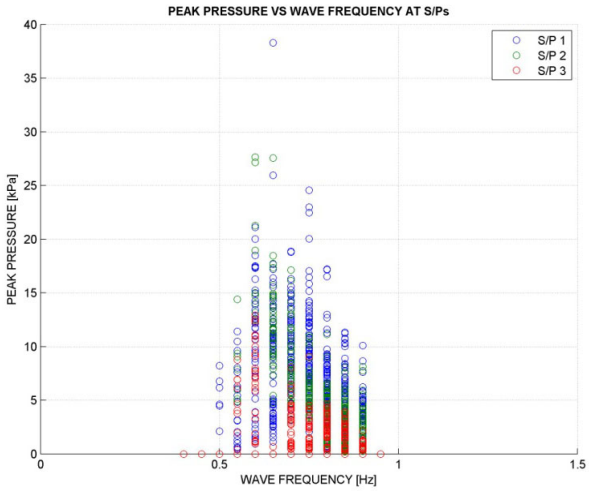

(b) P_p at S/P's

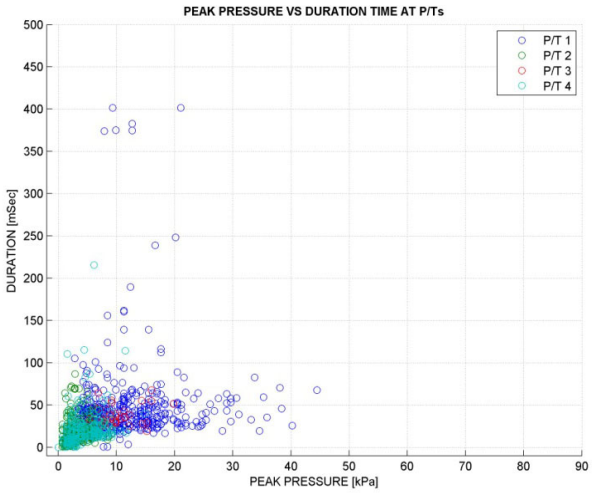

(c) P_p vs TD at P/T's

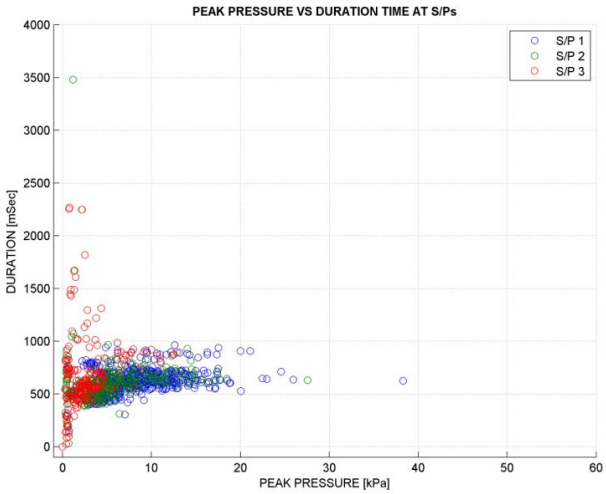

(d) P_p vs T_D at S/P's

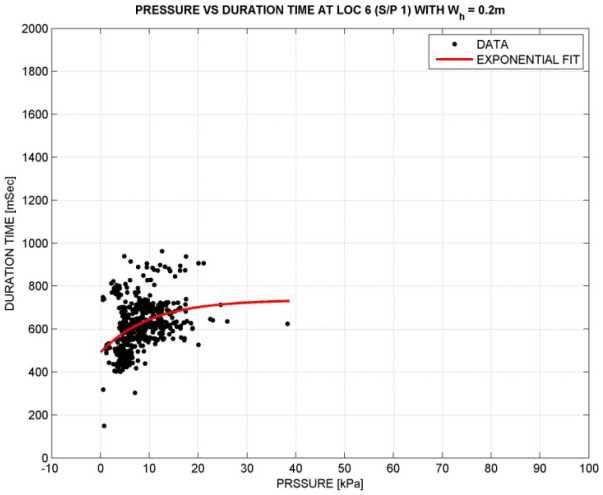

(e) P_p vs T_D at S/P 1

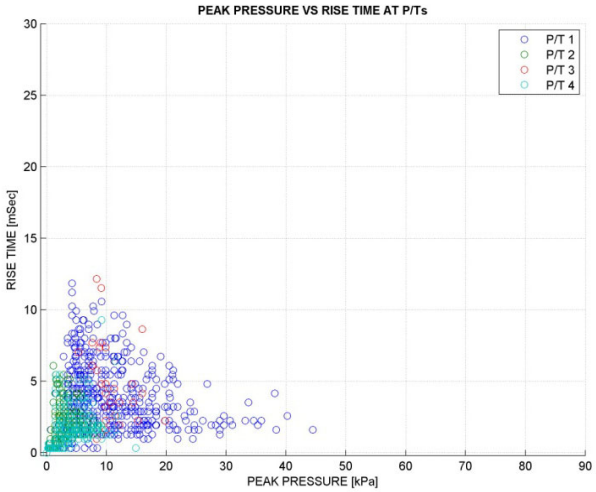

(f) T_R at P/Ts

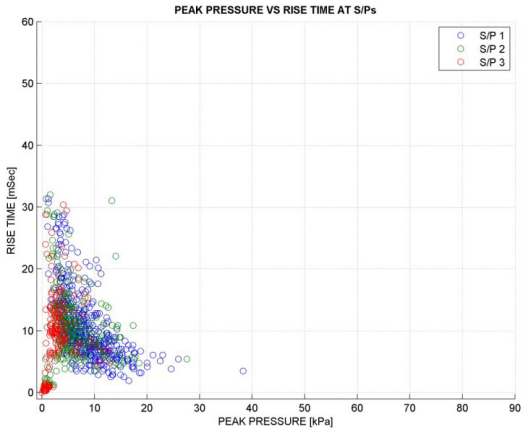

(g) T_R at S/P's

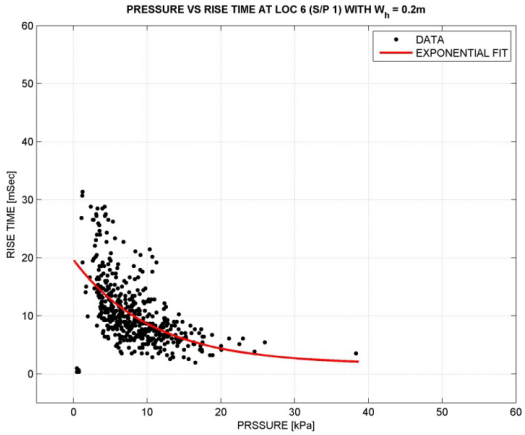

(h) T_R at S/P 1

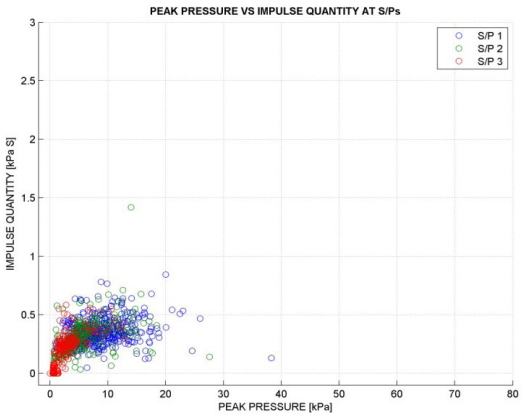

(i) Q_I at P/T's

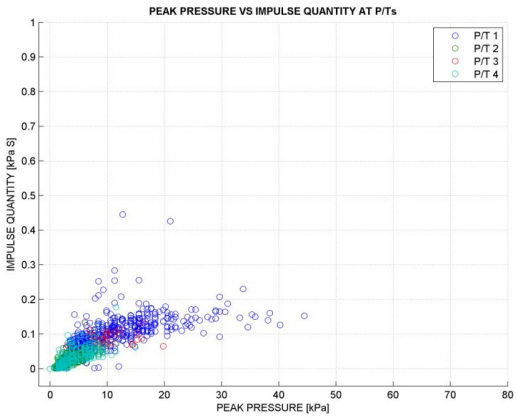

(j) Q_I at S/P's

Figure 14. Hydro-impact characteristics at all locations in the entire test matrix

Corresponding histograms and probability distributions (P/D) in the entire test matrix are shown in Figure 15. The pressure at slam patches 2 and 3 and the acceleration approach exponential distributions, which is the area where relatively lower pressure occurs. Note that the pressure 40 kPa in model scale corresponds to 280 kPa in full-scale based on Froude's law. The exceptionally high acceleration of 50 g in Figure 15 (h) is the response of the local structure. It must be noted that the local structure where the accelerometer is attached is in vacuo and was not investigated in this case; however, it is inferred that the excessive power up to higher frequency range contributes to this extraordinary acceleration.

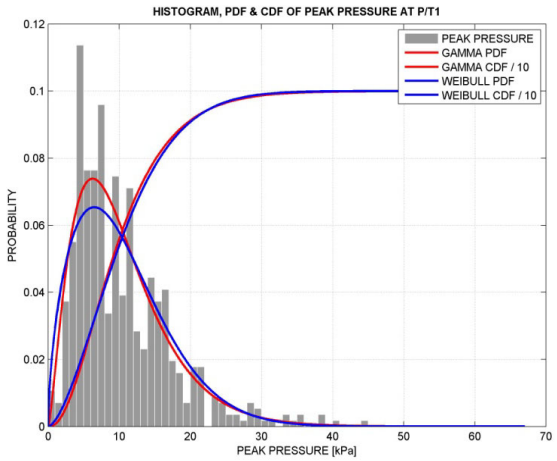

(a) Histogram and P/D at P/T 1

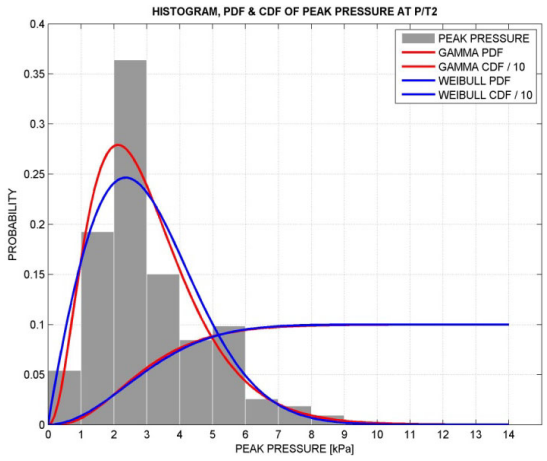

(b) Histogram and P/D at P/T 2

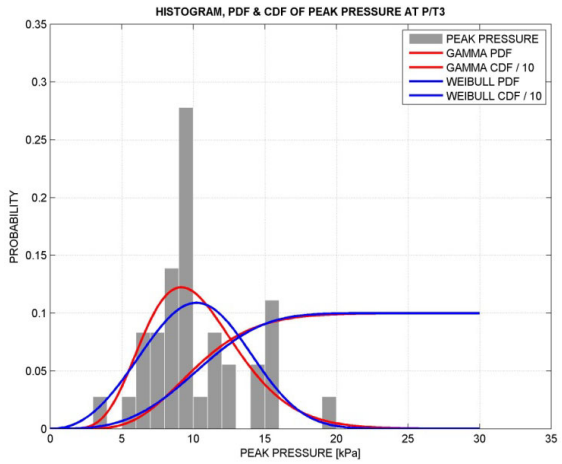

(c) Histogram and P/D at P/T 3

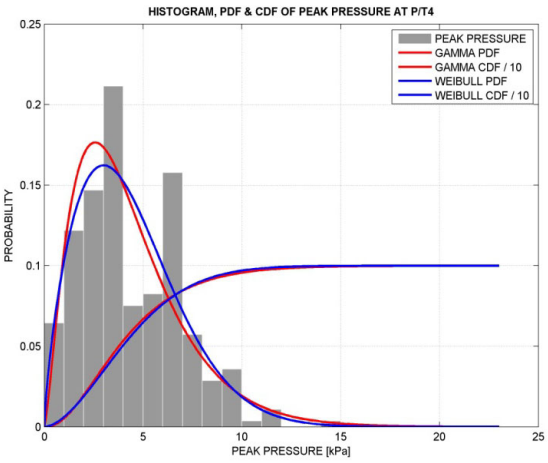

(d) Histogram and P/D at P/T 4

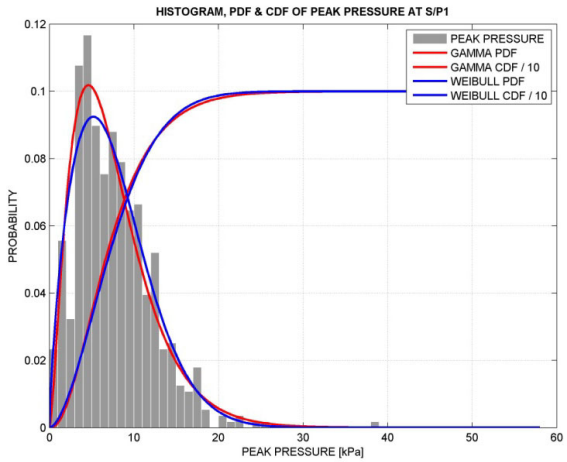

(e) Histogram and P/D at S/P 1

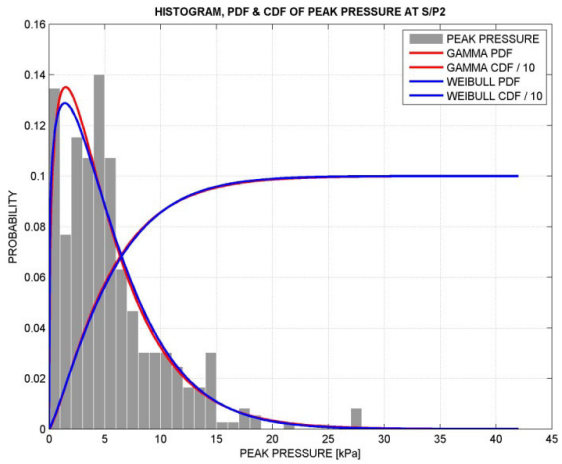

(f) Histogram and P/D at S/P 2

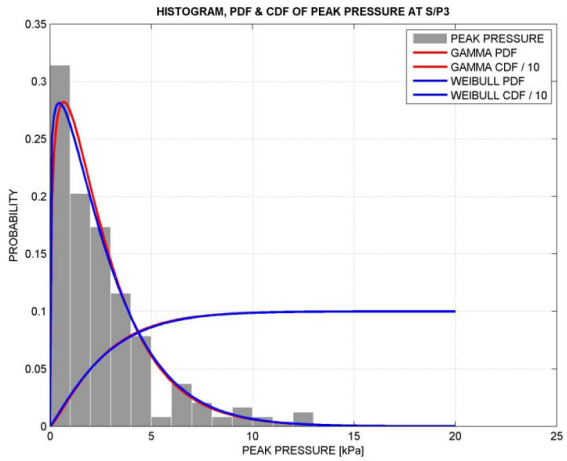

(g) Histogram P/D at S/P 3

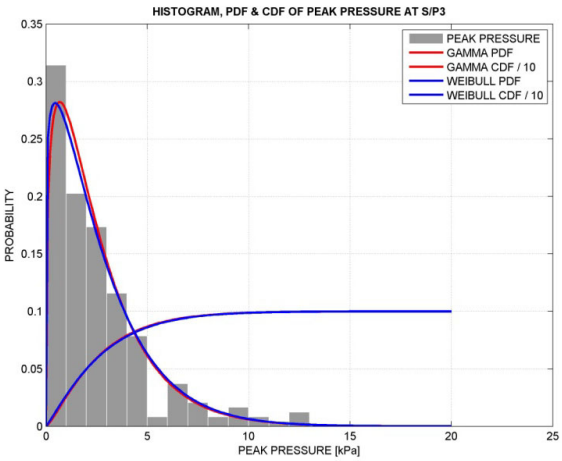

(h) Histogram P/D at Accelerations

Figure 15. Histogram and Histogram P/D at all locations in the entire test matrix

The extreme peak pressures (P_{EX}) are selected from each run and used in the calculation of the extreme value distribution. Figure 16 shows the extreme value distribution in which the concave start in the QQ plot suggests a Fréchet-type distribution. Extremely high peak pressures such as 80 kPa (which corresponds to 560 kPa in full-scale) can be expected with very low probability.

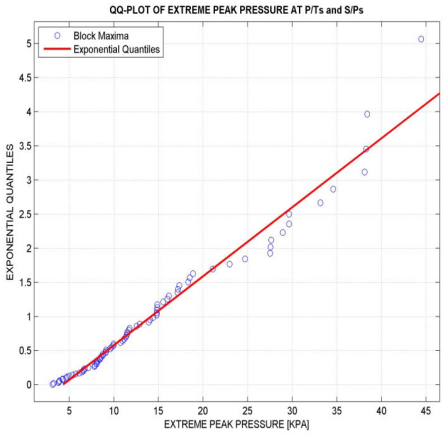

(a) QQ plot of PEX at P/T's and S/P's

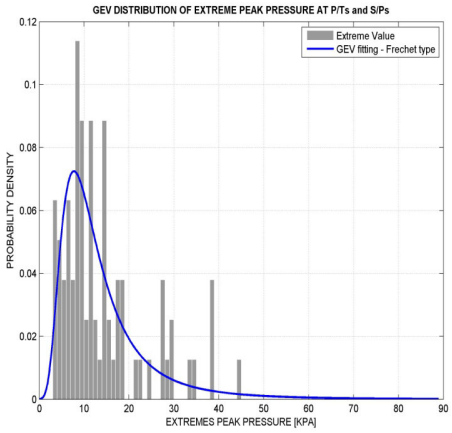

(b) Extreme value distribution (Fréchet-type)

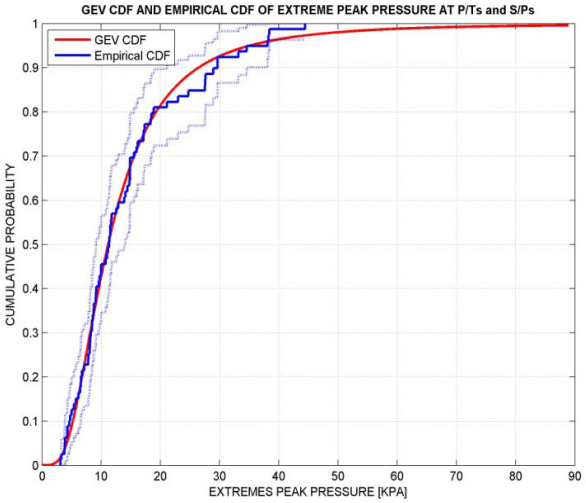

(c) CDF of extreme value

Figure 16. Extreme value distribution

NOTE ON SCALE METHODOLOGY

Scaling the test results up to full-scale is another challenge to solve. Since the boundary condition and natural behaviour of the slam patch are different from the hull plate of the prototype it is difficult to justify the use of the system. However, if reasonable assumptions can be made as described below, then the slam patch system represents a scale model of the hull plate of the prototype.

First of all, the slam patch system measures a force response to an external force. The measured force has two components; i.e., the net hydro-impact force and the structural response of the slam patch system itself. Segregation of the components of forces solely depends on the system's natural behaviour and the characteristics of the external force. In some of the drop test cases, because the measured data contains the structure's natural behaviour, it is difficult to separate the net hydro-impact force and structure's resonant response. However, by using a filtering process to eliminate the component of frequencies where resonance of the structure exists, the hydro-impact force can be estimated. In the

case of the seakeeping-slamming test, the response is mainly hydro-impact force because the frequency range is well below the structure's resonance range. It can therefore be justified to use the slam patch to measure the external hydro-impact load, slightly coupled with the structure's resonance.

Second, in this test, the first objective is to measure the hydro-impact force and the second is to find the hydro-elastic effect of the local structure under hydro-impact. So, to find the natural characteristics of the slam patch system, FRF of force transmissibility is plotted. If the force transmissibility between the model and prototype are assumed to be the same, Froude's law can be applied, where frequency is scaled as $1/\lambda^{1/2}$ and the force transmissibility remains the same. Here, the force transmissibility is receptance/receptance (Mead, 2000), where one familiar receptance used in naval architecture is the transfer function.

Furthermore, since the impulse has the dimensions of force and time, if the force is scaled by λ^3 or pressure by λ and time by $\lambda^{1/2}$, the quantity of (force) impulse can be scaled up by $\lambda^{7/2}$, or quantity of pressure impulse by $\lambda^{3/2}$. Further study may be needed to find the exact scale law for the hydro-impact and FSI problem so that Froude's law can be adapted to the hydro-impact problem.

TRANSIENT RESPONSE OF SIMPLE STRUCTURE

Carrying out the transient response of an Open 60 yacht under the hydro-impact based on the test results is left for further study. Before that, a simple structure is studied to give insight into the structural dynamics under an impulse. In this study, a cantilever beam and a simply supported plate under half-sine impulse are studied analytically and numerically.

A qualitative approach is tried to see the "relativity" between the structure's natural characteristics and the applied impulse load. An impulse is quantified by the shape of the impulse and its duration time and is a key factor in the calculation of the structure's transient response where the impulse is applied (Harris and Piersol, 2002). Since the shapes are varied in the test, it is difficult to determine the representative shape of the impulse and its duration time. This is left for further study. In this calculation, a half-sine function is employed to see the relativity.

Clamped beam

Two cases are of interest. One is where the relative time difference between the structure's first natural frequency and the duration time of the impulse is high, low and zero, respectively, by changing the Young's modulus of the material, and the other is by adding mass on the beam. To clarify the response easily, "clamped beam" is selected and simulated in the commercial finite element analysis program ANSYS™. The main parameters in this simulation are listed in Table 4 and Table 5.

Table 4. Parameter 1 - Changing the Young's modulus

Geometry	1 m × 0.05 m × 0.05 m
Young's modulus	2, 32, 128 GPa
Poisson's ratio	0.3
Density	2100 kg/m^3
Load magnitude	5000 N
Duration of impulse	5 ms
Impulse shape	Half sine
1st f_n of structure	50, 200, 500 Hz

Table 5. Parameter 2 - Adding mass

Geometry	1 m × 0.05 m × 0.05 m
Young's modulus	108.6 GPa
Poisson's ratio	0.35
Density	1700 kg/m^3
Added mass (per unit length)	0, 5, 10, 20, 30 kg
Load magnitude	5000 N
Duration of impulse	5 ms
Impulse shape	Half sine

The transient responses at the midpoint of the clamped beam with various Young's moduli are shown in Figure 17 and Table 6.

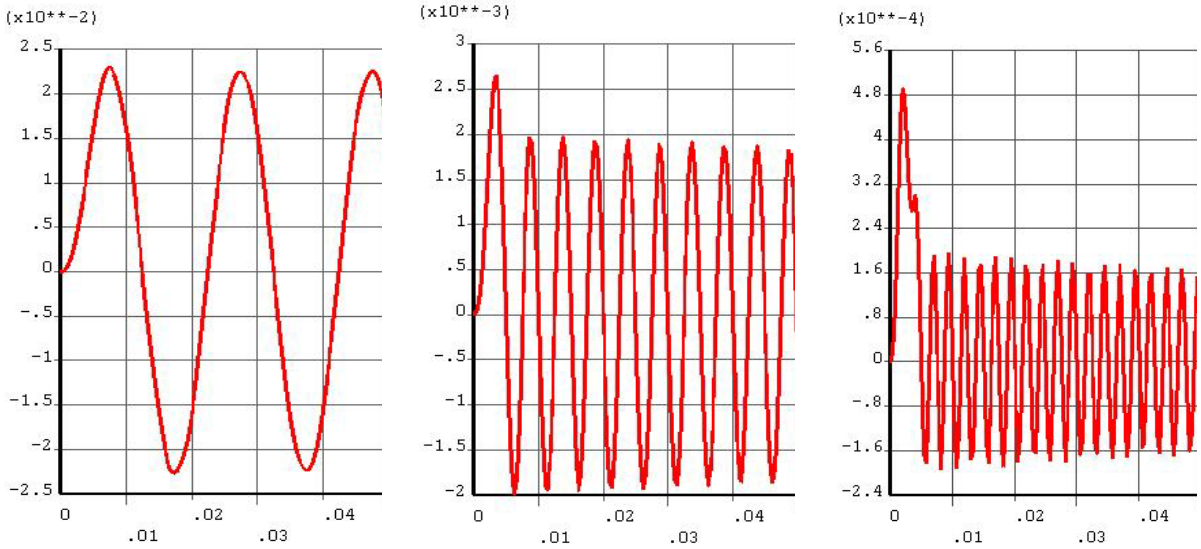

a) f_n =50 Hz b) f_n =200 Hz c) f_n =400 Hz

Figure 17. Deflections to half-sine impulse with various Young's moduli

Table 6. Responses at various Young's moduli

f_n	Static (mm)	Ratio to 50 Hz (%)	Transient (mm)	Ratio to static (%)
50	25.04	100	23.08	92
200	1.56	6.23	2.65	170
400	0.39	1.55	0.491	126

It can be seen from the results that when the relativity is zero (in this case f_n is 200 Hz and the duration time of impulse is 5 ms), the transient/static ratio (170%) is larger than the other cases (92% for f_n=50Hz and 126% for f_n=400 Hz). However, as the natural frequency of the structure increases, the responses to static and impulse loads significantly decreases.

The transient responses at the midpoint of the clamped beam with various added mass are shown in Figure 18 and Table 7.

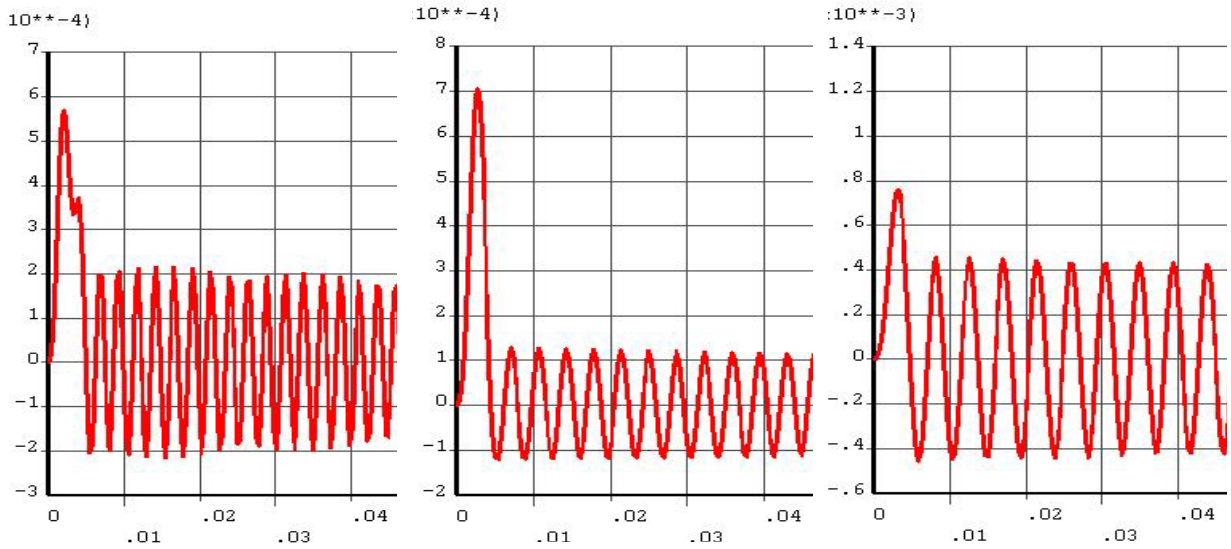

a) Mass = 0 kg **b) Mass = 5 kg** **c) Mass = 10 kg**

Figure 18. Deflections to half-sine impulse with various added mass

Table 7. Responses at various added mass

Added mass	f_n	Static (mm)	Transient (mm)	Ratio to static (%)
0	410	0.46	0.57	123
5	278	0.46	0.70	152
10	224	0.46	0.76	165

Similar results can be found such that as the added mass increases, f_n decreases. At the same time the transient deflection and the transient/static ratio also increase. Generally when a simple structure is in or on the water, because of the role of added mass of water, the natural frequency of the boat in terms of local and global structure decreases (Kwak, 1996; Ramachandra and Meyer-Piening, 1996).

As shown in Figure 17 and Figure 18, when the duration time of the impulse approaches the 1st natural period of the structure, the ratio of transient deflection to static deflection increases. This is what the structural designer of boat must avoid. Higher stiffness does not guarantee a safe hull unless the effect of the added virtual mass or the behaviour of the structure in wet mode under hydro-impact is known.

Simply supported plate

Firstly, a simply supported plate in dry mode under half-sine impulse (impulse pressure on the plate with half-sine shape in time domain) is studied. Using the modal superposition method and Duhamel's integral, an analytical solution of the transient response of a simply supported plate under half-sine impulse can be obtained. On the other hand, a numerical solution using the commercial finite element analysis code is found to compare well with the results to the analytical solution. Table 8 shows the comparison.

Table 8. Responses of a simply supported square plate

(a) Specification of calculation

Geometry	1 m × 1 m × 0.005 m
Material	Steel
Load magnitude	5 kPa
Duration of impulse	0.04, 0.1, 1 sec
Impulse shape	Half-sine
1st f_n of structure	50, 200, 500 Hz

(b) Natural frequency of the plate in Hz

Mode	Mode shape	Analytical	Numerical	Difference (%)
1	(1,1)	25.40	25.33	0.27
2	(1,2)	63.52	63.19	0.51
3	(2,1)	63.52	63.19	0.51
4	(2,2)	101.63	100.53	1.08

(c) Maximum deflections in mm to various loadings

	Maximum deflection (mm)		
Loading type	Analytical	Numerical	Difference (%)
Static	8.87	8.79	0.90
Dynamic (duration time=0.04 sec)	15.46	15.37	0.58
Dynamic (duration time =0.1sec)	9.75	9.99	2.40
Dynamic (duration time =1 sec)	9.03	9.04	0.11

So far, the calculation results are based on a relatively very simple structure. The structure of the boat is relatively complex, and it is expected that the local complexity (which means that the natural characteristics will be vary from area by area) will play an important role in the dynamic response in terms of deflection, stress or strain with or without the water.

CONCLUSIONS

Through this study, it was found that:

- A slam patch system can be used to measure the hydro-impact load and/or the local structure's response to an external load if well designed to represent the local structure in terms of force transmissibility.
- To segregate the components of the slam patch's response to the net hydro-impact load from the fluid and the resonant response of slam patch, the resonant frequencies of the slam patch must be well beyond the hydro-impact load range. On the other hand, in the case of trying to find the response that has a specific representative structure's natural characteristics from full-scale prototype, the slam patch must be designed and implemented in terms of the same transmissibility between the model and full scale.
- The natural frequencies in the dry mode are consistently decreased compared to the slam patch in wet mode.
- In the drop test, as drop height increases, the slam patch's measurement is consistently greater that the pressure transducer's because of the existence of the slam patch's natural characteristics of resonance. However, the possibility of the sampling rate problem still exists.
- In the seakeeping-slamming test, the measured force/pressure is far lower than the drop test result and since the measurement is well below the structure's resonance range, it can be said that the measurement is net hydro-impact load.
- Gamma and Weibull distributions show good agreement with the histograms.
- As the relativity between external impulse and natural behaviour of the structure approach zero, the transient response increases in terms of transient/static deflection ratio in the simple structures.
- Qualitatively, the local structures will respond to the external hydro-impact load as the slam patch responds.

Nonetheless, some recommendations for further research can be provided:

- The slam patch must be studied in further detail to overcome the resonant problem when the objective is to measure the net hydro-impact load.
- The wave matrix in the seakeeping-slamming test must reflect the real sea condition where the boat operates, for example, irregular waves, steep waves or higher wave height.
- The sampling rate must be re-considered over 20 kHz to investigate the accuracy of the hydro-impact pressure.

REFERENCES

ABS (1994). *Guide for building and classing offshore racing yachts*. American Bureau of Shipping.

Allen, R., Jones, R. and Taylor, D. (1978). "A simplified method for determining structural design limit pressures on high performance marine vehicles." *Proceedings of AIAA/SNAME Advanced Marine Vehicle Conference*, San Diego, CA.

Bunting, E. and Sheahan M. (2009). "Broken by design?" *Yachting World*, April, 66-79, IPC INSPIRE Ltd.

BV (2008). *Rules for the Classification and Certification of Yachts*. Bureau Veritas.

Campbell, I. and Weynberg, P. (1979). *Slam load histories on cylinders*, Technical report, WUMTIA, University of Southampton.

Faltinsen, O. (2000). "Hydroelastic slamming." *Journal of Marine Science and Technology*. 5(2), 49-65.

Harris, C., Piersol, A. (2002). *Harris' shock and vibration handbook*. McGraw-Hill.

Heller, S. and Jasper, N. (1961). "On the structural design of planing craft." *Transaction of RINA*, 103, 49-65.

Hentinen, M. and Holm, G. (1994). "Load measurement on the 9.4m sailing yacht sail lab." *13th International Symposium Yacht Design and Yacht Construction, Netherlands*, 131-161.

ISO (2008). *ISO 12215 Small craft – Hull construction and scantlings, Part 5: Design pressures for monohulls design stresses, scantlings determination*. International Organization for Standardization.

Joubert, P. (1982). "Strength of bottom plating of yachts." *Journal of Ship Research*, 26 (1), 45-49.

Joubert, P. (1996). "Tests on yacht hull plating." *Marine Technology*, 33, 130-140.

Kapsenberg, G., Veer, A., Hackett, J. and Levadou, M. (2003). "Aftbody slamming and whipping loads." *SNAME Annual Meeting*, 111, 213-231.

Kwak, M. (1996). "Hydroelastic vibration of rectangular plates." *Journal of Mechanics*, 63 (1), 110-115.

Kwon, S., Lee, Y., Sim, I., Kim, Y., Jung, J., Park, J., and Jang, T (2005), "Experimental study on sloshing for large LNGC design." *Proceedings of the fifteenth International Offshore and Polar Engineering Conference*, Seoul, Korea.

Manganelli, P., Wagemakers, B. and Wilson, P. (2003). "Investigation of slamming loads using slam patches on a scaled model of an Open 60' class yacht." *International Journal of Small Craft Technology*, 145, 47-62.

Manganelli, P. (2006). *Experimental investigation of dynamic loads on offshore racing yachts*. Ph.D thesis, University of Southampton, UK.

Mead, D (2000). *Passive vibration control*. John Wiley & Sons.

Ochi, M. and Motter, L. (1973). "Prediction of slamming characteristics and hull responses for ship design." *Transactions of SNAME*, 81, 144-176.

Ramachandra, L., and Meyer-Piening, H. (1996). "Technical note - Transient response of sandwich plates in contact with water." *Computer & Structure,* 60(4), 677-681.

Reichard, R. (1984). “The structural response of small craft to dynamic loading.” *Proceedings of the 14th AIAA Symposium on the Aero/Hydronautics of Sailing*, 30, 105-110.

Savitsky, D. and Brown, P. (1976). “Procedures for hydrodynamic evaluation of planing hulls in smooth and rough water.” *Marine Technology*, 13(4), 381-400.

Stavovy, A. and Chuang, S. (1976). “Analytical determination of slamming pressures for high-speed vehicles in waves.” *Journal of Ship Research*, 20(4), 190-198.

von Karman, T. (1929). *The impact on seaplane floats during landing - Technical report*. Aerodynamical Institute of the Technical High School, Aachen.

Wraith, W. (1998). *Pressure loads on ship hull plating caused by slamming*. Ph.D thesis, University of Melbourne, Australia.